ORIGINAL PAPER

Modeling the antiferromagnetic $Mn^{II}Mn^{II}$ system within the protein phosphatase-5 catalytic site

E. A. Salter · R. E. Honkanen · A. Wierzbicki

Abstract Protein phosphatase-5 (PP5), a novel target for inhibition in a search for new antitumor drugs, contains a homobimetallic $Mn^{II}Mn^{II}$ system in its catalytic site. The ground electronic state is an antiferromagnetically-coupled singlet. We report optimizations of a known inhibitor within a 42-residue model of the PP5 catalytic site under several two-level hybrid ONIOM computational models. Using the high-resolution crystal structure of a PP5/inhibitor complex as reference, we compare geometric parameters as the qualities of the "high-level" and "low-level" wavefunctions are successively improved by using the correct antiferromagnetic (AF) singlet state. We find that the UB3LYP AF wavefunction for the high-level region is necessary for experimental fidelity. A closed-shell semi-empirical method (RPM6) can be used for the low-quality part of the hybrid scheme to afford geometries which are qualitatively on par with that obtained using the more time-consuming open-shell UB3LYP AF wavefunction. As the AF state can be elusive for such a large system, the ferromagnetic (F) state can also be used in the low-quality calculations without impacting the geometry.

Keywords Antiferromagnetic bimetal system · DFT · Enzyme-inhibitor interactions · ONIOM · Protein phosphatase-5

E. A. Salter · A. Wierzbicki (✉)
Department of Chemistry, University of South Alabama, Mobile, AL 36688, USA
e-mail: awierzbicki@southalabama.edu

R. E. Honkanen
Department of Biochemistry & Molecular Biology, University of South Alabama, Mobile, AL 36688, USA

Introduction

Serine/threonine protein phosphatase 5 (PP5; *PPP5C*) is a member of the PPP family of protein phosphatases. PP5 is expressed in most, if not all, mammalian tissues, and elevated PP5 expression correlates with the development of breast cancer, notably invasive ductile carcinoma with metastases [1]. Selective PP5 inhibition is thus a design goal for the development of probe molecules, which will be useful to study the roles of PP5 in biology and disease. Specific inhibitors of PP5 may also serve as lead compounds for antitumor drug development [2]. Currently our understanding of PP5 suggests over expression in cancer cells aids tumor progression by suppressing hypoxia and genomic stress-induced apoptosis [1, 3–5]. At present there is no known selective inhibitor of PP5, chiefly because of its high structural similarity with other PPP-family enzymes.

Our current aim is to construct a computational model for the PP5 catalytic site to be used in making effective modifications of norcantharidin (1), Fig. 1, a known inhibitor of PP5, PP1, and PP2A ($IC_{50} \approx 1$–9 μM), in pursuit of greater PP5 potency and selectivity. The PP5 catalytic site contains a bimetal system essential to the catalytic hydrolysis of the phosphate ester bond of substrate proteins. The bimetal system has been identified as a pair of Mn^{2+} ions, about 3.2 Å apart [6]. We propose that the ground electronic state of this system is an antiferromagnetically-coupled open-shell singlet state with five electrons "up" on one metal and five electrons "down" on the other. Antiferromagnetic coupling for the $Mn^{II}Mn^{II}$ system was observed long ago in the EPR spectrum of manganese-substituted phosphotriesterase [7]. Small $Mn^{II}Mn^{II}$-based complexes can be successfully modeled using quantum methods [8], and how to use system "fragments" to setup initial guesses for successful SCF convergence is the subject of a Gaussian technical note [9]. Obtaining the correct antiferromagnetic (AF) electronic state
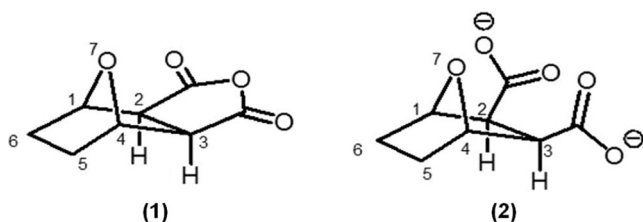
Fig. 1 Norcantharidin (1) and its hydrolyzed form, endothall (2)

is nevertheless difficult, particularly in large systems intended to approximate actual protein environments. For our stated purpose, the model system must span at least 40–50 residues of the catalytic domain to include PP5-specific features, which may afford selectivity. Here, we assess several two-level hybrid computational schemes to determine if it is necessary to use wavefunctions that reflect the true electronic configuration in both the high- and low-level regions, or if proper treatment is needed only in the high-level region.

Density functional theory (DFT) methods and hybrid DFT methods have been commonly used in past studies of manganese-centered biological mechanisms; sometimes the high-spin ferromagnetic (F) state of the bimetal system has been used for convenience, as the energetic effect of the coupling is small and essentially constant from reactants to products [10, 11]. Recently, Ribeiro et al. [12] studied the catalytic mechanism of PP5 using DFT on a "cluster" model of the catalytic site with phosphoserine as substrate. Their evaluation of several spin states concluded that the AF electronic configuration is the more stable one. Also, Das et al. [13] have carried out DFT calculations to study the mechanism of a functioning enzyme complex, designed as a representation of the active site of the purple acid phosphatase from sweet potato. The active site therein contains an $Fe^{III}Mn^{II}$ system — isoelectronic to the system of interest here, and its most stable electronic state is the AF singlet.

The crystal structure of the PP5/(1) complex has been determined by x-ray diffraction analysis (pdb entry 3H61)

[14]. The bound form of (1) is the dianion of the bisacid known as endothall (2), Fig. 1, where the anhydride functionality has been hydrolyzed. Figure 2 shows a close-up view of the binding position of (2) within the small depression containing the catalytic $Mn^{II}Mn^{II}$ bimetal system. Endothall is seated tightly within this recession, and its carboxylates are directly coordinated to the Mn^{2+} ions and to functional groups of nearby residues, Fig. 2b. Endothall's bridge oxygen (O7) is also directly coordinated to one of the metal ions (Mn^R). The presumptive nucleophile in PP5-mediated catalysis is a hydroxide ion which bridges the two metal ions in the unliganded enzyme [6, 12]. This bridge hydroxide ion is not seen in the PP5/(1) crystal structure, either having been consumed or displaced. Waters of hydration of bimetal system are also displaced by the inhibitor.

Here, we report optimizations of (2) within a fixed model of the PP5 catalytic site to test various two-level hybrid computational models in which, at minimum, the high-level employs the all-electron B3LYP DFT method. We compare optimized geometric parameters as the qualities of the "high-level" and "low-level" wavefunctions are successively improved by using the correct AF singlet state.

Methods

A 42-residue model of the PP5/(2) system (overall charge=+ 1), Fig. 2, was built from the crystal structure [14] using Gaussview (v5.0, Semichem, Inc.). Where the peptide backbone was broken, carboxylates are terminated as aldehydes and amines are unprotonated. Acidic/basic residue side chains were protonated/deprotonated as appropriate for pH=7; all histidines in the model were chosen to be neutral, with the exception of His^{304}, which was protonated, as its basicity is presumably enhanced by the proximity of the carboxylate of Asp^{274}. The crystal structure contains no hydrogen atoms; thus, the positions of all hydrogens were determined in a

Fig. 2 ONIOM computational model of the PP5/endothall system and atom labeling. (**a**) High-level and low-level regions of the hybrid scheme are shown in tube and wireframe, respectively. Hydrogen atoms are not shown. (**b**) Close-up view of endothall's important interactions within the catalytic site
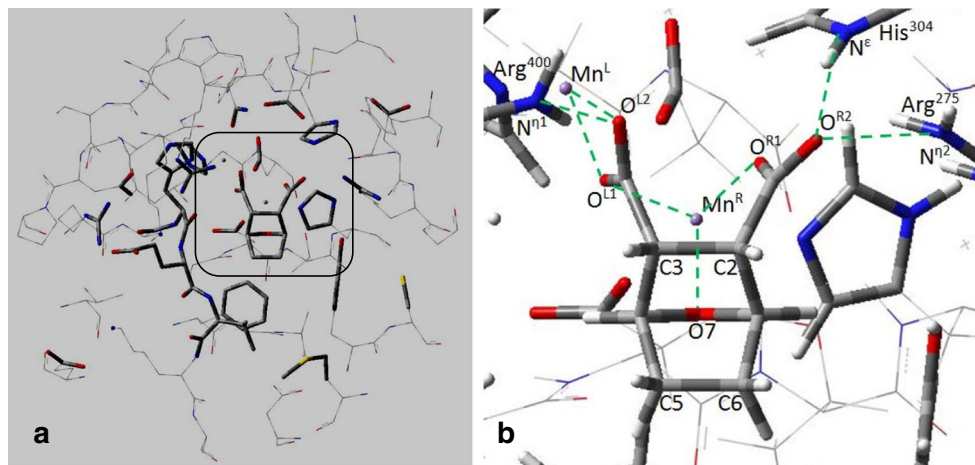
pre-optimization using the semi-empirical PM6 method [15] implemented in Gaussian09 [16].

Five two-level ONIOM [17] optimizations with varying treatments of the antiferromagnetic $Mn^{II}Mn^{II}$ system (Table 1) were carried out using Gaussian09 [16]. The high-level wavefunction was determined by the B3LYP DFT method [18–21], commonly used for such systems, with the modest 6-31G(d) (or 6-31G(d,p)) basis set [22–24]. The low-level regions were either determined by the semi-empirical PM6 method [15] or by the B3LYP method with the CEP-4G basis [25, 26] and associated effective core potentials. Model I employs simple closed-shell wavefunctions for both high (RB3LYP) and low levels (RPM6). Model II uses the correct AF wavefunction for the high-level calculation for comparison with model I. Model III tests the use of the F wavefunction at the low level with the correct AF wavefunction at the high level, while model IV employs the correct AF wavefunction at both levels. Model V is included as a test of the impact of p functions on the hydrogen atoms with respect to model IV. Guess fragments were selected to set up UB3LYP convergence to the intended AF (singlet) or F (undecet) unrestricted open-shell states; Gaussian09 does not permit use of guess fragments for the PM6 method. Only the endothall ligand was allowed to move during the optimizations. The default SCRF option for water as solvent was used.

The high-level region, common to all four models and shown in Fig. 2a (tube), was chosen to include the two Mn^{2+} ions and all coordinated functional groups, endothall and portions of several residues in contact with it, and all other charged functional groups in the 42-residue model. (Note: additional side chains were also included in the high-level region.) Under the hybrid scheme, where a high-level atom is bonded to a low-level atom, the latter is replaced by a terminal hydrogen atom in the high-level calculation. Figure 3 shows a close up view of the $Mn^{II}Mn^{II}$ system and the coordinated functional groups contained within the high-level region.

Table 1 Two-level ONIOM computational models[a]

	High-quality	Low-quality
I	RB3LYP/6-31G(d) (S)	RPM6 (S)
II	UB3LYP/6-31G(d) (AF)	RPM6 (S)
III	UB3LYP/6-31G(d) (AF)	UB3LYP/CEP-4G (F)
IV	UB3LYP/6-31G(d) (AF)	UB3LYP/CEP-4G (AF)
V	UB3LYP/6-31G(d,p) (AF)	UB3LYP/CEP-4G (AF)

[a] AF, antiferromagnetic singlet state; F, ferromagnetic 11-et (undecet) state; S, closed-shell singlet state. All models include the default SCRF = (solvent = water) option of Gaussian09 to simulate the presence of water at the system boundary. The ONIOM system energy is determined from low-quality (lq) and high-quality (hq) energies: E = E_3(system, lq) - E_1(high-level region, lq)+E_2(high-level region, hq)
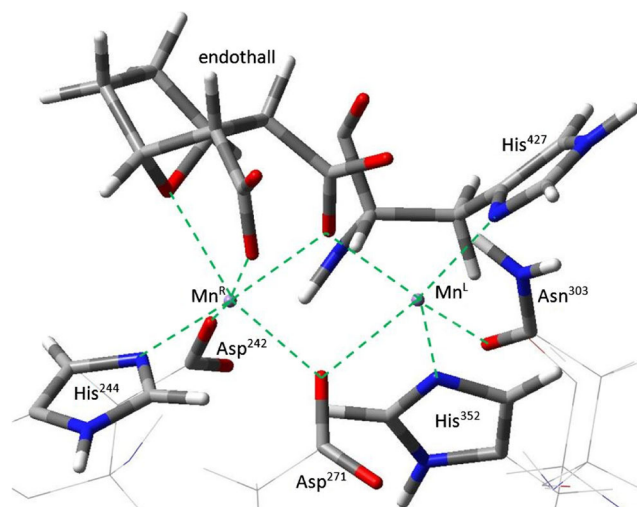

Fig. 3 Close-up of the $Mn^{II}Mn^{II}$ system in the PP5/endothall ONIOM model. High- and low-level regions of the hybrid scheme are shown in tube and wireframe, respectively. Mn^R and Mn^L have six and five coordinations, respectively. In calculations for the high-level region, endothall and His^{427} are fully included, the asparates 271 and 242 are approximated as formate ions, the histidines 244, 352, and 427 are included as imidazole molecules, and Asn^{303} is included as a formamide molecule

Results

The selection of two guess fragments, one containing Mn^R and endothall, the other containing Mn^L and the rest of the system, proved successful in converging to the intended spin states under quadratic convergence (SCF=XQC option); the states were confirmed by inspection of the Mulliken spin populations of the two Mn^{2+} ions, with +4.8/−4.8 as typical values obtained for the AF state and +4.8/+4.8 for the F state. These values are within the 5.0±0.2 absolute range cited for Mn(II) [10] and are close to the values reported by Ribeiro et al. [12] for the similar, substrate-bound system. Selected optimized parameters for our different hybrid schemes are provided in Table 2, along with values from the x-ray crystal structure; the corresponding interaction distances are illustrated in Fig. 2b. Included in Table 2 are three dihedral angles; the first two indicate positioning of endothall relative to the bi-metal system, the third indicates strain on the endothall scaffold.

Discussion

Table 2 shows that model I, with restricted closed-shell treatments for both high- and low-quality wavefunctions, poorly reproduces the ligand-Mn^{2+} interactions. Moreover, in the high-level calculation of model I, the Mulliken charges for Mn^R (+0.97) and Mn^L (+1.12) of +0.97 are respectively 10 % and 5 % lower than in the other models. Notably, the r(O7-Mn^R), r(O^{L2}-Mn^L) and r(O^{L1}-Mn^R) distances for model I are

Table 2   Selected geometric parameters of the PP5/endothall system[a]

	r(O7-Mn^R)	r(O^{L1}-Mn^L)	r(O^{L2}-Mn^L)	r(O^{L1}-Mn^R)	r(O^{R1}-Mn^R)	r(O^{L2}-N^b)	r(O^{R2}-N^c)	r(O^{R2}-N^d)	d(Mn^L,Mn^R, C3,C5)	d(Mn^L,Mn^R, C3,C2)	d(C3,C2, C6,C5)
I	2.087	1.987	2.493	2.008	2.052	3.188	2.664	3.244	143.4	−130.8	−5.7
II	2.390	2.082	2.965	2.205	2.278	2.838	2.739	2.958	140.5	−132.8	−4.3
III	2.394	2.114	2.993	2.202	2.258	2.810	2.749	3.019	141.5	−131.8	−4.0
IV	2.395	2.114	2.993	2.202	2.258	2.810	2.749	3.019	141.5	−131.8	−4.0
V	2.393	2.114	2.996	2.206	2.254	2.801	2.736	3.030	141.6	−132.4	−3.8
expt[e]	2.29	2.03	2.97	2.23	2.21	2.86	2.72	3.11	140.3	−132.7	2.4

[a] Atom labels given in Fig. 2b. Models defined in Table 1. Distances (r) are in Å; dihedral angles (d) are in degrees

[b] N$^{\eta 1}$ of Arg^{400}. [c] N$^{\varepsilon}$ of His^{304}. [d] N$^{\eta 2}$ of Arg^{275}. [e] Experimental data from pdb entry 3H61, resolution 1.45 Å

0.20, 0.48, and 0.22 Å shorter than the respective experimental values. These shortened distances place the endothall scaffold under some strain (d(C3,C2,C6,C5)= −5.7° versus +2.4°) and causes the O^{L2}-N$^{\eta 1}$(Arg^{400}) interaction distance to be too long by 0.33 Å. When the high-level region is treated properly using the AF wavefunction (models II-V), better positioning of (2) is achieved, with better overall agreement with experimental interaction distances, including excellent agreement for the aforementioned O^{L2}-Arg^{400} distance (model II: 2.838 Å versus 2.86 Å). The geometric parameters obtained for models II-V are very similar; the introduction of the F (or AF) wavefunctions in the low-level calculations of models III and IV offer little, if any, improvement in structure, but do provide electronic stability. The parameters obtained for models III and IV are essentially identical, showing that the F treatment for the low-level calculations may provide a useful alternative to the proper AF treatment. Little improvement is observed in the addition of polarization functions on the hydrogen atoms in going from model IV to V.

In the hybrid scheme, the system energy is estimated by combining two low-quality (lq) energies and one high-quality (hq) energy: E=E$_3$(system, lq) - E$_1$(high-level region, lq)+ E$_2$(high-level region, hq). Consequently, a common electronic description is important to achieve cancellation in the energetics of the Mn^{II}Mn^{II} system as incorporated in the values of E$_3$ and E$_1$. We have experienced energy shifts during model II-based optimizations of new test inhibitors; when this happens, the unstable electron density shifts in either the calculation of E$_1$ or E$_3$ and proper cancellation cannot be expected. So although the RPM6 can be used for the low-quality calculations and affords geometries which are qualitatively the same as the more time-consuming AF (or F) treatment under the UB3LYP method, model II is not expected to be generally reliable for the next step in assessing new inhibitor modifications (i.e., the estimation of relative binding energies). In contrast, the AF and F states are confirmed as electronically stable. We add that the F and AF states are essentially degenerate (uncorrected for magnetic coupling) with the AF lower by <0.01 kcal mol^{-1} (B3LYP/6-311(d,p), high-level region).

While the AF state can be elusive, particularly for the whole system in the E$_3$ calculation, the F state can in some cases be more easily obtained. Thus, model III could provide an alternative to model IV in optimizations of proposed (1)-based inhibitors. Either optimization can be followed with a single-point calculation employing a better basis set for an improved estimate of relative binding energy.

Conclusions

We have carried out optimizations of (2) [the hydrolyzed form of (1)] within a large, 42-residue, fixed model of the PP5 catalytic site (Fig. 2) to test various two-level ONIOM hybrid DFT-based computational models (Table 1). Using the solved crystal structure of the PP5/(1) complex as reference, we have compared geometric parameters as the qualities of the "high-level" and "low-level" wavefunctions are successively improved by using the antiferromagnetic (AF) singlet state corresponding to the lowest-energy electronic configuration of PP5's Mn^{II}Mn^{II} bimetal system. A closed-shell representation of the high-level region (model I) was found to give unacceptable binding parameters, Table 2. When the high-level region was treated using the stable and correct AF wavefunction (models II-V), better positioning of (2) was achieved, including excellent agreement with the observed inhibitor-Mn^{2+} and inhibitor-residue interaction distances. The geometric parameters obtained for models III and IV (using the F and AF wavefunctions respectively for the low-quality calculations) are essentially identical, Table 2. We conclude that the F wavefunction for the low-level calculations can serve as a useful alternative to the proper AF wavefunction, without impacting the geometry.

References

1. Golden T, Aragon IV, Rutland B, Tucker JA, Shevde LA, Samant RS, Zhou G, Amable L, Skarra D, Honkanen RE: Elevated levels of Ser/Thr protein phosphatase 5 (PP5) in human breast cancer. Biochim Biophys Acta 2008.

2. McConnell JL, Wadzinski BE (2009) Targeting protein serine/threonine phosphatases for drug development. Mol Pharmacol 75: 1248–1261

3. Golden T, Swingle M, Honkanen RE (2008) The role of serine/threonine protein phosphatase type 5 (PP5) in the regulation of stress-induced signaling networks and cancer. Cancer Metastasis Rev doi: 10.1007/s10555-008-9125-z

4. Morita K, Saitoh M, Tobiume K, Matsuura H, Enomoto S, Nishitoh H, Ichijo H (2001) Negative feedback regulation of ASK1 by protein phosphatase 5 (PP5) in response to oxidative stress. Embo J 20: 6028–6036

5. Zhou G, Golden T, Aragon IV, Honkanen RE (2004) Ser/Thr protein phosphatase 5 inactivates hypoxia-induced activation of an apoptosis signal-regulating kinase 1/MKK-4/JNK signaling cascade. J Biol Chem 279:46595–46605

6. Swingle MR, Honkanen RE, Ciszak EM (2004) Structural basis for the catalytic activity of human serine/threonine protein phosphatase-5. J Biol Chem 279:33992–33999

7. Chae MY, Omburo GA, Lindahl PA, Raushel FM (1993) Antiferromagnetic coupling in the binuclear metal cluster of manganeses-substituted phosphotriesterase. J Am Chem Soc 115: 12173–12174

8. Mitani M, Katsurada T, Wakamatsu Y, Yoshioka Y (2005) Density functional study on the highest and lowest spin states of $[Mn_2O_2(H_2O)_8]^{q+}$ ($q = 0, 2, 4$). Internet Electron J Mol Des 4:94–105

9. Modeling Antiferromagnetic Coupling in Gaussian 09. [http://www.gaussian.com/g_tech/afc.htm]

10. Siegbahn PE (2002) Quantum chemical studies of manganese centers in biology. Curr Opin Chem Biol 6:227–235

11. Siegbahn PE (2001) A quantum chemical study of the mechanism of manganese catalase. Theor Chem Acc 105:197–206

12. Ribeiro AJM, Alberto ME, Ramos MJ, Fernandes PA, Russo N (2013) The catalytic mechanism of protein phosphatase 5 established by DFT calculations. Chem Eur J 19:14081–14089

13. Das B, Daver H, Singh A, Singh R, Haukka M, Demeshko S, Meyer F, Lisensky G, Jarenmark M, Himo F, Nordlander E (2014) A heterobimetallic $Fe^{III}Mn^{II}$ complex of an unsymmetrical dinucleating ligand: a structural and functional model complex for the active site of purple acid phosphatase of sweet potato. Eur J Inorg Chem 2014: 2204–2212

14. Bertini I, Calderone V, Fragai M, Luchinat C, Talluri E (2009) Structural basis of serine/threonine phosphatase inhibition by the archetypal small molecules cantharidin and norcantharidin. J Med Chem 52:4838–4843

15. Stewart JPP (2007) Optimization of parameters for semiempirical methods. V. Modification of NDDO approximations and application to 70 elements. J Mol Model 13:1173–1213

16. Frisch MJ, Trucks GW, Schlegel HB, Scuseria GE, Robb MA, Cheeseman JR, Scalmani G, Barone V, Mennucci B, Petersson GA et al. (2009) Gaussian 09, revision A.1. Gaussian Inc, Wallingford, CT

17. Dapprich S, Komáromi I, Byun KS, Morokuma K, Frisch MJ (1999) A new ONIOM implementation in gaussian 98. 1. The calculation of energies, gradients and vibrational frequencies and electric field derivatives. J Mol Struct (Theochem) 462:1–21

18. Becke AD (1993) Density-functional thermochemistry. III. The role of exact exchange. J Chem Phys 98:5648–5652

19. Lee C, Yang W, Parr RG (1998) Development of the Colle-Salvetti correlation-energy formula into a functional of the electron density. Phys Rev B 37:785–789

20. Stephens PJ, Devlin FJ, Chabalowski CF, Frisch MJ (1994) Ab initio calculation of vibrational absorption and circular dichroism spectra using density functional force fields. J Phys Chem 98:11623–11627

21. Vosko SH, Wilk L, Nusair M (1980) Accurate spin-dependent electron liquid correlation energies for local spin density calculations: a critical analysis. Can J Phys 58:1200–1211

22. Ditchfield R, Hehre WJ, Pople JA (1971) Self-consistent molecular orbital methods. 9. Extended Gaussian-type basis for molecular-orbital studies of organic molecules. J Chem Phys 54:724–728

23. Hehre WJ, Ditchfield R, Pople JA (1972) Self-consistent molecular orbital methods. 12. Further extensions of Gaussian-type basis sets for use in molecular-orbital studies of organic-molecules. J Chem Phys 56:2257–2261

24. Rassolov VA, Pople JA, Ratner MA, Windus TL (1998) 6-31G* basis set for atoms K through Zn. J Chem Phys 109:1223–1229

25. Stevens WJ, Basch H, Krauss M (1984) Compact effective potentials and efficient shared-exponent basis-sets for the 1st-row and 2nd-row atoms. J Chem Phys 81:6026–6033

26. Stevens WJ, Krauss M, Basch H, Jasien PG (1992) Relativistic compact effective potentials and efficient, shared-exponent basis-sets for the 3rd-row, 4th-row, and 5th-row atoms. Can J Chem 70: 612–630